Acta Pharmaceutica Sinica B 2025;15(5):2498−2510

Chinese Pharmaceutical Association
Institute of Materia Medica, Chinese Academy of Medical Sciences

Acta Pharmaceutica Sinica B

www.elsevier.com/locate/apsb
www.sciencedirect.com

ORIGINAL ARTICLE

Anti-SARS-CoV-2 prodrug ATV006 has broad-spectrum antiviral activity against human and animal coronaviruses

Tiefeng Xu[a,†], Kun Li[d,†], Siyao Huang[a,†], Konstantin I. Ivanov[b], Sidi Yang[b], Yanxi Ji[a], Hanwei Zhang[a], Wenbin Wu[a], Ye He[h], Qiang Zeng[a], Feng Cong[e], Qifan Zhou[f], Yingjun Li[c,f], Jian Pan[a], Jincun Zhao[b,c], Chunmei Li[a], Xumu Zhang[f,g], Liu Cao[a,*], Deyin Guo[a,b,c,d,*]

[a]*Centre for Infection and Immunity Studies (CIIS), School of Medicine, Shenzhen Campus of Sun Yat-sen University, Guangzhou 518107, China*
[b]*Guangzhou Laboratory, Bio-island, Guangzhou 510320, China*
[c]*State Key Laboratory of Respiratory Diseases, National Clinical Research Center for Respiratory Diseases, Guangzhou Institute of Respiratory Health, the First Affiliated Hospital of Guangzhou Medical University, Guangzhou 510182, China*
[d]*Institute of Human Virology, Department of Pathogen Biology and Biosecurity, and Key Laboratory of Tropical Disease Control of the Ministry of Education, Zhongshan School of Medicine, Sun Yat-sen University, Guangzhou 510080, China*
[e]*Guangdong Province Key Laboratory of Laboratory Animals, Guangdong Laboratory Animals Monitoring Institute, Guangzhou 510663, China*
[f]*Shenzhen Key Laboratory of Small Molecule Drug Discovery and Synthesis, Department of Chemistry, Shenzhen Grubbs Institute and Medi-X Pingshan, Southern University of Science and Technology, Shenzhen 518000, China*
[g]*Medi-X Pingshan, Southern University of Science and Technology, Shenzhen 518118, China*
[h]*Guangdong Provincial Key Laboratory of Malignant Tumor Epigenetics and Gene Regulation, Guangdong-Hong Kong Joint Laboratory for RNA Medicine, Medical Research Center, Sun Yat-sen Memorial Hospital, Sun Yat-sen University, Guangzhou 510120, China*

Received 14 October 2024; received in revised form 25 December 2024; accepted 14 January 2025

*Corresponding authors.
E-mail addresses: guodeyin@mail.sysu.edu.cn (Deyin Guo), caoliu@mail.sysu.edu.cn (Liu Cao).
[†]These authors made equal contributions to this work.
Peer review under the responsibility of Chinese Pharmaceutical Association and Institute of Materia Medica, Chinese Academy of Medical Sciences.

https://doi.org/10.1016/j.apsb.2025.02.028

KEY WORDS

Broad-spectrum antiviral activity;
SARS-CoV-2;
RNA-dependent RNA polymerase (RdRp);
Human coronaviruses;
Animal coronaviruses;
Oral bioavailability;
Antiviral therapy;
In vivo

Abstract Coronavirus-related diseases pose a significant challenge to the global health system. Given the diversity of coronaviruses and the unpredictable nature of disease outbreaks, the traditional "one bug, one drug" paradigm struggles to address the growing number of emerging crises. Therefore, there is an urgent need for therapeutic agents with broad-spectrum anti-coronavirus activity. Here, we provide evidence that ATV006, an anti-SARS-CoV-2 nucleoside analog targeting RNA-dependent RNA polymerase (RdRp), has broad antiviral activity against human and animal coronaviruses. Using mouse hepatitis virus (MHV) and human coronavirus NL63 (HCoV-NL63) as a model, we show that ATV006 has potent prophylactic and therapeutic activity against murine coronavirus infection *in vivo*. Remarkably, ATV006 successfully inhibits viral replication in mice even when administered 96 h after infection. Due to its oral bioavailability and potency against multiple coronaviruses, ATV006 has the potential to become a useful antiviral agent against SARS-CoV-2 and other circulating and emerging coronaviruses in humans and animals.

1. Introduction

The coronavirus disease 2019 (COVID-19) pandemic, caused by severe acute respiratory syndrome coronavirus 2 (SARS-CoV-2)[1], has affected nearly 777 million people and caused over 7.1 million deaths as of Feb 2025 (https://covid19.who.int/). Coronaviruses (CoVs) are a large family of enveloped positive-sense single-stranded RNA viruses[2], named for their crown-like appearance under the electron microscope. Human coronaviruses include severe acute respiratory syndrome coronavirus 2 (SARS-CoV-2), Middle East respiratory syndrome-associated coronavirus (MERS-CoV)[3], severe acute respiratory syndrome coronavirus (SARS-CoV), human coronavirus 229E (HCoV-229E), human coronavirus OC43 (HCoV-OC43), human coronavirus NL63 (HCoV-NL63), and human coronavirus HKU1 (HCoV-HKU1)[4]. In the last two decades, at least two known animal coronaviruses have jumped to humans: novel canine coronavirus (CCoV-HuPn-2018)[5] and porcine deltacoronavirus (PDCoV)[6]. Most importantly, three human coronaviruses—SARS-CoV, MERS-CoV, and SARS-CoV-2—have caused global epidemics in the 21st century[7-10]. Therefore, broad-spectrum antivirals are urgently needed to meet the challenges of current and future coronavirus outbreaks.

The RNA-dependent RNA polymerase (RdRp) of SARS-CoV-2 plays an essential role in the viral life cycle, is conserved across coronaviruses, and represents a promising target for anti-coronavirus drug discovery[11-13]. Several inhibitors of SARS-CoV-2 RdRP have been identified, including remdesivir[13,14], molnupiravir[15,16], VV116[17], azvudine[18] and ATV006[19]. Importantly, remdesivir can inhibit the replication of several pathogenic RNA viruses, including respiratory syncytial virus (RSV), Ebola virus (EBOV), and epidemic and epizootic CoVs[20-23]. The same is true for molnupiravir, which is effective against influenza virus, EBOV and CoVs[22,24,25]. Thus, RdRp inhibitors have the potential to be used as broad-spectrum antivirals.

ATV006 was first discovered in our laboratory[19] and is currently in Phase III clinical trials (Clinical Trials Identifier: NCT05715528). We have previously shown that it can effectively inhibit the replication of SARS-CoV-2 and its variants *in vitro* and *in vivo*[19]. In this study, we demonstrate that ATV006 has potent *in vitro* activity against multiple coronaviruses, including HCoV-229E, HCoV-OC43, HCoV-NL63, and six epizootic coronaviruses. Additionally, we demonstrate that both prophylactic and therapeutic administration of ATV006 reduces viral replication and lung damage in MHV-infected mice. Furthermore, we also validated the efficacy of ATV006 in HCoV-NL63-infected mice, where we observed significant inhibition of viral replication and a reduction in lung inflammation. These findings suggest that ATV006 is a broad-spectrum antiviral agent and a promising candidate for clinical trials against various human and animal coronaviruses.

2. Materials and methods

2.1. Compounds, cell lines, and viruses

Compounds (remdesivir, GS-441524, ATV006) were synthesized in-house, purified by HPLC for >95% purity. Remdesivir was prepared as 5 mg/mL with 12% sulfobutylether-β-cyclodextrin (pH 3.5−4.0). GS-441524 was in 0.5% sodium carboxymethyl cellulose in water. ATV006 was in 5% Solutol HS-15 and 20% 1,2-propanediol, diluted with double-distilled water.

MHV-A59 experiments were in the ABSL-2 lab at Guangdong Laboratory Animals Monitoring Institute. Animal study protocols were approved by the Animal Welfare Committee and followed guidelines of the Animal Care and Use Committee (Approval number: I-IACUC2020001). Details on cells and viruses used are in Supporting Information Table S1.

2.2. Assays for anti-human coronaviruses activity

Cells were plated at 20,000 cells per well in 96-well plates 24 h before infection. ATV006 and GS-441524 were diluted in 100% DMSO to achieve a dose range from 0.01 to 50 μmol/L. All experiments were performed in triplicate. Cells were infected with HCoV-OC43 (MOI = 0.01), HCoV-229E (MOI = 0.01), or HCoV-NL63 (MOI = 0.05), depending on the cell line, and cultured at 33 °C for 2−7 days. Supernatants or cells were then collected for qRT-PCR analysis. Dose−response curves were generated by plotting viral RNA copies against drug concentrations using GraphPad Prism 8.0. Details on viruses and cells are in Table S1, and qPCR primers are listed in Supporting Information Table S2.

2.3. Assays for anti-animal coronaviruses activity

Cells were seeded in 48-well plates and cultured for 24 h until they reached approximately 90% confluence. After three washes

with serum-free medium, cells were infected with the virus at an MOI of 0.01 at 37 °C for 1 h. Next, medium with dilutions of ATV006 or DMSO was added. After a 48 h incubation at 37 °C, both cells and supernatants were collected for viral load determination *via* qRT-PCR. The EC_{50} values were derived from the dose−response curve. Details on the viruses and cells are in Table S1, and the qPCR primers are listed in Table S2[26].

2.4. Quantitative reverse transcription polymerase chain reaction (qRT-PCR) analysis

RNA was extracted using the Viral RNA Kit (OMEGA, GA, USA). For quantifying tissue RNA, total RNA was extracted from tissue samples using the GoldHi Plasmid Mini Kit (CWBIO, Beijing, China) as per the manufacturer's instructions. The absolute quantification of MHV-A59 RNAs were performed by HiScript® II U + One Step qRT-PCR Probe Kit (Vazyme Biotech, Nanjing, China) using MHV-A59 probe. Simultaneously, mRNAs were reverse transcribed into cDNA using the PrimeScript RT reagent Kit (Takara, Kyoto, Japan) to measure relative mRNA expression. Gapdh was used as the reference gene for normalization *via* the ΔCt method. qRT-PCR primers are listed in Table S2.

2.5. Mouse models of MHV infection

As outlined in a previous report[27], BALB/c mice, which were obtained from SPF biotechnology (Beijing, China), were mildly anesthetized with isoflurane and intranasally infected with MHV-A59 in 40 μL DMEM or intraperitoneal injection with MHV-A59 in 100 μL DMEM. The animals were humanely euthanized by cervical dislocation, and blood samples were collected from the orbital artery and orbital vein[28]. The lungs and livers were then harvested. Subsequently, the left lobe of lungs and the left lateral lobe of livers were fixed in 4% paraformaldehyde. The other lungs and livers were divided equally and then bathed in PBS or TRIzol reagent for additional analyses. MHV-A59 infection experiments took place in the Biosafety Level 2 (BSL 2) lab at Guangdong Laboratory Animals Monitoring Institute. Protocols were approved by the Animal Welfare Committee (Approval number: I-IACUC2020001), and procedures followed Animal Care and Use Committee guidelines.

2.6. Mouse models of HCoV-NL63 infection

Eight-week-old female H11-K18-hACE2 (C57BL/6JGpt) mice were obtained from GemPharmatech Co., Ltd. For HCoV-NL63 infection experiments in K18-hACE2 mice, the animals were intranasally inoculated with 4×10^5 PFU of the virus. Following infection, the mice were humanely euthanized *via* cervical dislocation, after which the lungs were harvested. The left lung lobe and the left lateral lobe of the liver were fixed in 4% paraformaldehyde. The remaining lung and liver tissues were evenly divided and either preserved in PBS or treated with TRIzol reagent for further analysis. All infection experiments were conducted in the Animal Biosafety Level 2 (ABSL-2) laboratory at the Guangzhou National Laboratory. The experimental protocols were reviewed and approved by the Animal Welfare Committee and adhered to the guidelines of the Institutional Animal Care and Use Committee (Application No. GZLAB-AUCP- 2023-11-A2).

2.7. MHV-A59 plaque assay

L2 cells were cultured in 100-mm dishes to 80%−90% confluence and then infected with virus dilutions ranging from 10^{-1} to 10^{-8}. After a 2 h incubation at 37 °C, the inoculum was removed, and cells were overlaid with 0.8% methyl cellulose in DMEM with 2% FBS for 1−2 days. For plaque staining, cells were treated with 0.5% crystal violet. After 6−8 h, stained plaques were counted[27].

2.8. Histopathology

For hematoxylin and eosin (H&E) staining, mouse lung sections were fixed in zinc formalin, embedded in paraffin, and sliced into 4 μm sections. These sections were stained with H&E, counterstained with hematoxylin (Hubei BIOSSCI Biotech Co., Ltd.), and mounted with neutral resin (Solarbio, Beijing, China). Images were scanned using a NanoZoomer S360. Liver inflammation and necrosis were graded using the HAI modified ISHAK score, evaluating necrosis and portal inflammation on a severity scale from 0 to 4. Additionally, an inflammatory score assessed alveolar hyperemia, hemorrhage, septal thickness, and neutrophil infiltration, also graded from 0 to 4[29].

2.9. AST/ALT assay

After incubation at room temperature to allow clotting, blood samples were centrifuged to separate the serum. The serum levels of alanine aminotransferase (ALT) and aspartate aminotransferase (AST) were measured using kits from Nanjing Jiancheng Bioengineering Institute[30].

2.10. Sequence analysis

The RdRp proteins of the coronavirus were aligned using mafft software and visualized using texshade software[31].

2.11. PK study in rat

Male SD rats (180−220 g, $n = 3$) were deprived of food for 12 h prior to drug administration[19]. ATV006 was given intravenously at a dosage of 4 mg/kg or intragastrically at a dosage of 20 mg/kg. The collection intervals are as follows: for intravenous administration at 0.083, 0.25, 0.5, 1, 2, 4, 8, and 24 h; for intragastric administration at 0.25, 0.5, 1, 2, 4, 6, 8, and 24 h[32]. Blood samples will be taken *via* the submandibular vein or another suitable vein, 30 μL per time point. Sample will be placed in tubes containing K_2-EDTA and stored on ice until centrifuged. The blood samples will be centrifuged at $6800 \times g$ for 6 min at 2−8 °C within 1 h after collected and stored frozen at approximately −70 °C[33]. The concentration of analytes in each sample was analyzed by LC/MS/MS.

2.12. Phylogenetic analysis

Amino acid sequences of the RdRp gene from various coronaviruses were aligned using Clustal X for sequence comparisons. Phylogenetic trees were constructed with the neighbor-joining algorithm in MEGA7.0.26 software. The tree was constructed proportionally, with branch lengths representing evolutionary distances between sequences analyzed. Statistical confidence in nodes was assessed through 1000 bootstrap replicates, and branches with

bootstrap values below 50% were condensed. Reference sequences, retrieved from the National Center for Biotechnology Information databases, are denoted by their reference numbers: SADS (AVM80464.1), SARS-CoV-2 (UHE05272.1), SARS-CoV (ACZ72150.1), MERS-CoV (QLD98007.1), HCoV-OC43 (AGT51429.1), HCoV-229E (QRK03801.1), HCoV-NL63 (WDE19040.1), CCoV-HuPn-2018 (QVL91810.1), PDCoV (ANI85845.1), MHV (NP_045299.2), CCoV (AEQ61967.2), FIPV (AAY32594.1), PEDV (QED40666.1), SADS (AVM80464.1), and TGEV (NP_058422.1).

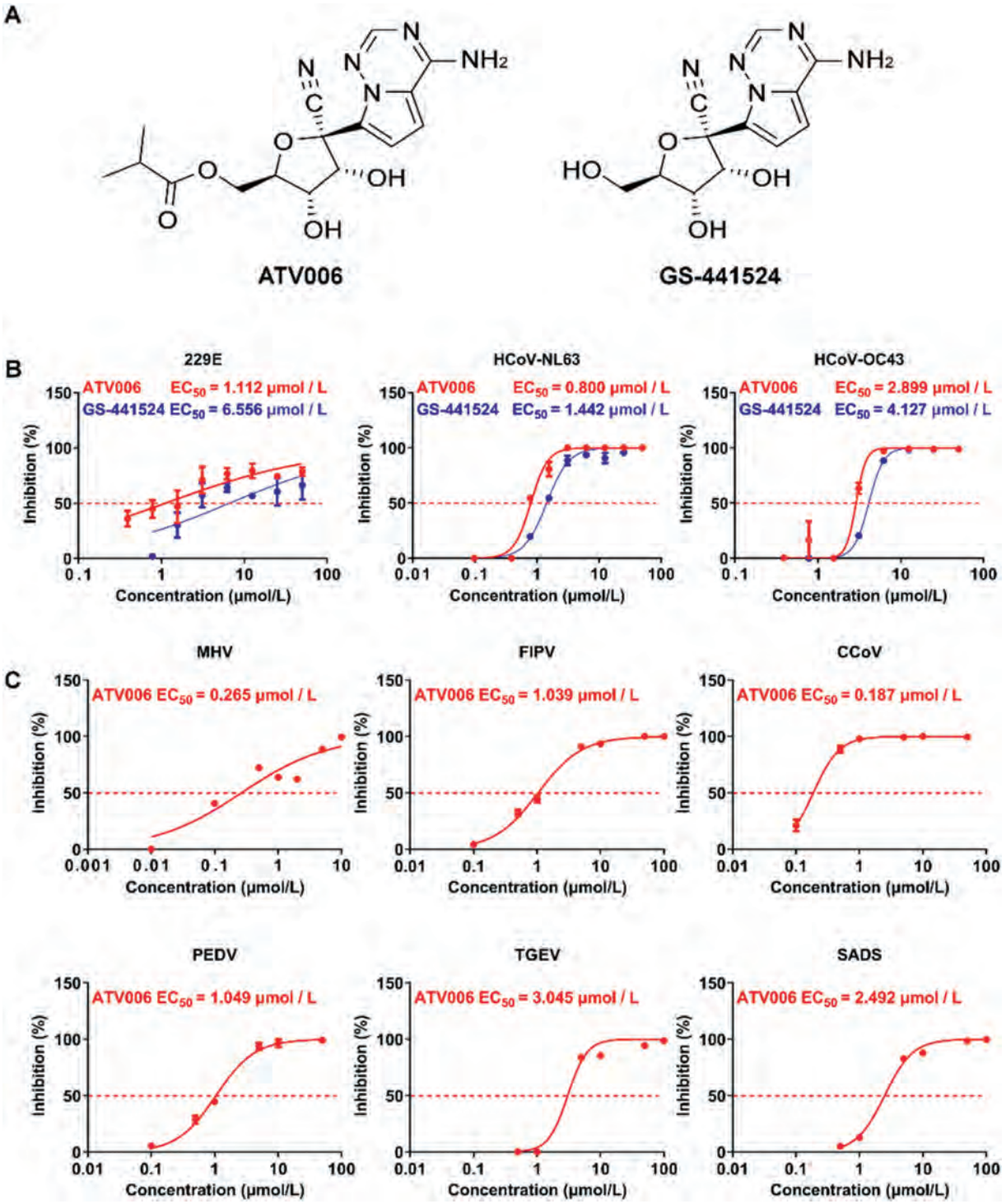

Figure 1 ATV006 has broad-spectrum antiviral activity against human and animal coronaviruses in cultured cells. (A) The chemical structures of ATV006 and GS-441524. Dose−response curves and EC_{50} values of ATV006 and GS-441524 against HCoV-229E, HCoV-NL63, and HCoV-OC43 (B) and ATV006 against MHV, FIPV, CCoV, PEDV, TGEV, and SADS (C). Detailed information on cell lines and virus strains is provided in Supporting Information Table S1. The data are expressed as mean ± standard error of mean (SEM).

2.13. Statistical analysis

All statistical data analyses were performed in GraphPad Prism 8. Statistical significance for each endpoint was determined using specific statistical tests. For data comparisons at a single time point, either the Kruskal−Walli's test or one-way ANOVA was used, accompanied by the appropriate multiple comparison test. A P value of <0.05 was considered significant for all tests. The specific tests used are indicated in each figure legend.

3. Results

3.1. ATV006 has broad-spectrum activity against human and animal coronaviruses

We have previously shown that the adenosine analog prodrug ATV006 has high oral bioavailability in rats and cynomolgus monkeys and has potent antiviral activity against several SARS-CoV-2 variants of concern (VOCs)[19]. In this study, we investigated the antiviral activity of ATV006 in cell culture against a variety of human and animal coronaviruses[34,35], and the chemical structures of ATV006 and its parent compound GS-441524 are shown in Fig. 1A. ATV006 had an EC_{50} of 2.899 μmol/L for HCoV-OC43, 1.122 μmol/L for HCoV-229E, and 0.800 μmol/L for HCoV-NL63 (Fig. 1B). Consistent with the findings for SARS-CoV-2[19], ATV006 demonstrated greater potency against human coronaviruses than GS-441524 (Fig. 1B).

ATV006 also demonstrated good antiviral activity against epizootic coronaviruses, including mouse hepatitis virus (MHV), feline infectious peritonitis virus (FIPV), porcine epidemic diarrhea virus (PEDV), canine coronavirus (CCoV), transmissible gastroenteritis virus (TGEV), and swine acute diarrhea syndrome coronavirus (SADS-CoV). All of these viruses are alphacoronaviruses, with the exception of MHV, which is a betacoronavirus. The EC_{50} values obtained were 0.265 μmol/L for MHV, 1.039 μmol/L for FIPV, 0.187 μmol/L for CCoV, 1.049 μmol/L for PEDV, 3.045 μmol/L for TGEV, and 2.492 μmol/L for SADS-CoV (Fig. 1C). These results indicate that ATV006 has broad-spectrum anti-coronavirus activity.

3.2. Oral ATV006 protects mice from death in the MHV infection model

To provide *in vivo* support for the *in vitro* findings that ATV006 has broad-spectrum antiviral activity, we tested its efficacy against MHV in mice. MHV can infect the lungs and livers of mice *via* intranasal inoculation, resulting in fatal outcomes[36]. Therefore, MHV is considered a good model virus for coronavirus research. ATV006 showed favorable pharmacokinetic data when administered intragastric and by injection (Table 1 and Supporting Information Fig. S1). ATV006 had an oral bioavailability (F%) of up to 98% after 20 mg/kg administration in rats, with a half-life of 3.62 ± 0.61 h. Supporting Information Fig. S2A illustrates our protocol for validating MHV infection. Two to five days after intranasal inoculation with MHV, viral titers in the lungs and liver increased significantly (Fig. S2B), as did levels of interferon and inflammatory cytokines (Fig. S2C). These results confirmed the successful establishment of the MHV infection model.

Our next goal was to find the lowest oral dose of ATV006 that could protect MHV-A59-infected mice from death and weight loss. The experimental timeline is shown in Fig. 2A. ATV006 effectively prevented mortality and weight loss in mice at doses ranging from 5 to 50 mg/kg. However, mice treated with 2 mg/kg ATV006 began to die at the 4th day post-infection (dpi) and all died by 10 dpi (Fig. 2B). Intraperitoneal (IP) administration of remdesivir (20 mg/kg) and oral administration of GS-441524 (50 mg/kg) similarly prevented MHV-infected mice from dying (Fig. 2B), but the body weight of the mice was lower than that of mice treated with ATV006 (50 mg/kg) (Fig. 2C). In contrast, all mice in the control group died at 7 dpi, while treatment with 2 mg/kg ATV006 prolonged survival and reduced viral titers in the liver by approximately sixfold. Notably, ATV006 at 50 mg/kg reduced viral titers by 1,000,000-fold and no live virus was found in the liver (Fig. 2D and E).

Table 1 Pharmacokinetic profile of ATV006 in Sprague−Dawley (SD) rats[a].

Parameter	Rat	
	IV (4 mg/kg)	IG (20 mg/kg)
AUC_{last} (μg/L·h)	2347 ± 354	11445 ± 813
$t_{1/2}$ (h)	1.30 ± 0.24	3.62 ± 0.61
T_{max} (h)	0.083	0.83 ± 0.29
C_{max} (μg/L)	3030 + 451	4017 ± 359
F (%)	−	98%

[a]$n = 3$, ATV006 was administered *via* the indicated route, and the parameters were calculated based on the results of the LC−MS/MS analysis of GS-441524. IV, intravenous; IG, intragastric.

3.3. Prophylactic administration of ATV006 inhibits MHV replication in vivo

MHV primarily infects the mouse liver and causes hepatitis. Therefore, we next evaluated the prophylactic effect of ATV006 in the liver. Supporting Information Fig. S3A schematically represents the experimental time course. We administered ATV006 along with intrahepatic MHV inoculation and analyzed viral abundance in the liver three days later using qRT-PCR and plaque assays. qRT-PCR analysis revealed that the levels of MHV genomic RNA (gRNA) and subgenomic RNA (sgRNA) were significantly reduced in the ATV006-treated group (10 and 50 mg/kg) compared to the vehicle group (Fig. S3B and S3C). Furthermore, plaque assay results showed that viral titers were below the detection limit in the ATV006-treated group (Fig. S3D). Serum levels of the liver injury markers alanine aminotransferase (ALT) and aspartate aminotransferase (AST) were also lower in the ATV006-treated group than in the control group (Fig. S3E). Using histopathological analysis and measurement of inflammatory factors, we found that ATV006 treatment resulted in a significant reduction in inflammatory cell infiltration (Fig. S3F) and caused a significant decrease in the expression of various inflammatory cytokines in the liver (Fig. S3G).

Pathogenic coronaviruses frequently cause respiratory infections[37]. Over the past two decades, coronaviruses with lung tropism have been responsible for three major human disease outbreaks: SARS, MERS, and COVID-19. In light of this, MHV is useful as a model of coronavirus infection in the lung, as it successfully infects the respiratory tract of mice[36]. Therefore, we next investigated the prophylactic effect of ATV006 in preventing lung MHV infection (Fig. 3A). Following the intranasal MHV challenge, the control group gradually lost weight starting at 2 dpi.

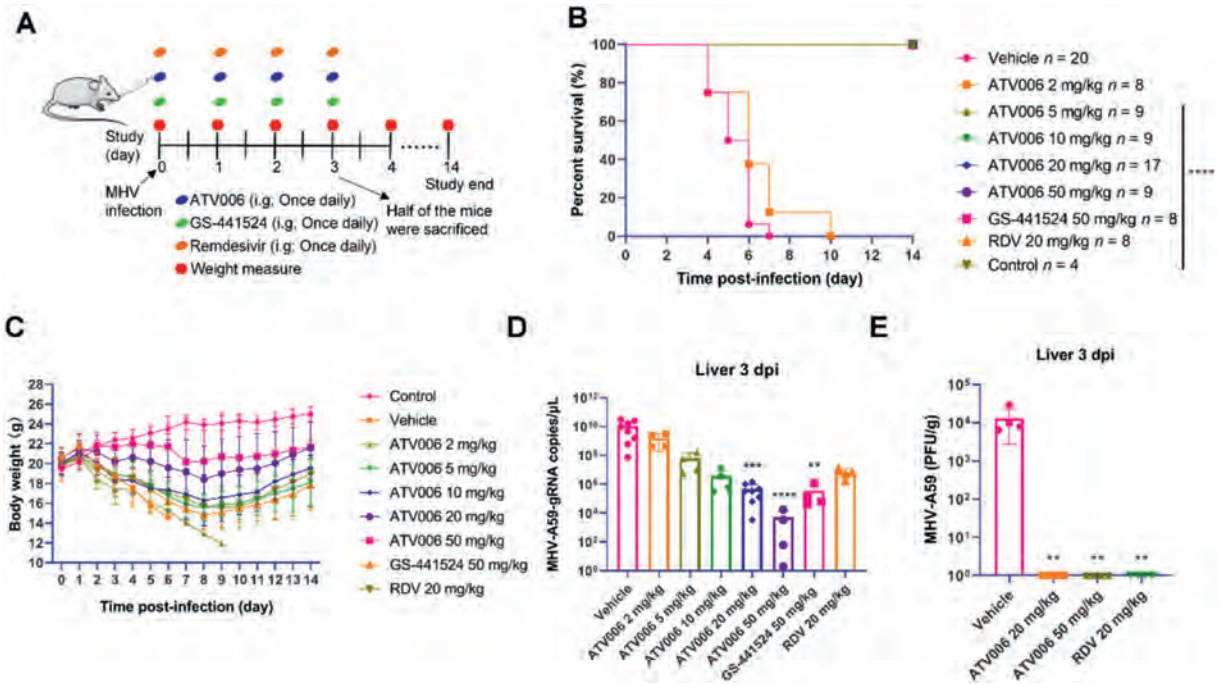

Figure 2 Antiviral activities of ATV006, remdesivir, and GS-441524 in MHV-infected mice. BALB/c mice were intranasally inoculated with 4×10^5 PFU of MHV-A59 and divided into the following groups depending on treatment: vehicle ($n = 20$), ATV006 (50, 20, 10, 5, or 2 mg/kg, administered intragastric once daily, $n = 8-17$), remdesivir (RDV, 20 mg/kg, administered by intraperitoneal injection once daily, $n = 8$), GS-441524 (50 mg/kg, administered intragastric once daily, $n = 8$), and a no-intervention control ($n = 4$). Half of the mice were euthanized at 3 dpi for analysis, and the remaining mice were monitored for survival, with the experiment terminating at 14 dpi. (A) The time course of the experiment. (B) The survival curve. (C) The change in mouse body weight over time after infection. (D, E) Viral abundance in the liver at 3 dpi as determined by qRT-PCR and plaque assay. The data are expressed as mean ± SEM, $^{**}P < 0.01$; $^{***}P < 0.001$; $^{****}P < 0.0001$ compared to the vehicle.

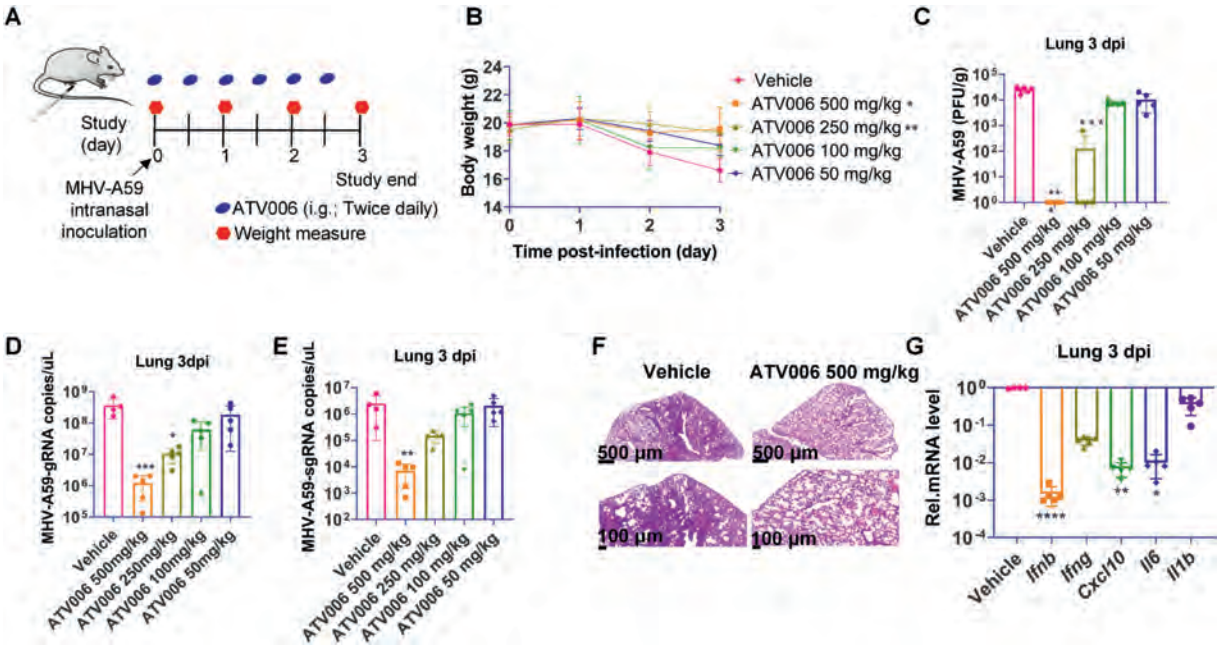

Figure 3 Prophylactic treatment of mice with ATV006 inhibits MHV replication. BALB/c mice were intranasally inoculated with 4×10^5 PFU of MHV-A59 and divided into the following groups depending on treatment: vehicle ($n = 6$) and ATV006 (500, 250, 100, or 50 mg/kg, administered intragastric twice daily, $n = 5$). (A) The time course of the experiment. (B) The change in mouse body weight over time after infection. (C–E) Viral abundance in the lung at 3 dpi as determined by qRT-PCR and plaque assay. (F) Histopathological analysis of lung tissues from the vehicle group and the ATV006-treated group (500 mg/kg intragastric, twice daily). (G) Representative chemokine and cytokine levels in the lung for the indicated groups at 3 dpi. The data are expressed as mean ± SEM, $^{*}P < 0.05$; $^{**}P < 0.01$; $^{***}P < 0.001$; $^{****}P < 0.0001$ compared to the vehicle.

However, combining the MHV challenge with ATV006 administration at doses ranging from 50 to 500 mg/kg did not result in the same weight loss (Fig. 3B). At 3 dpi, we assessed the abundance of MHV in the lungs of the mice using qRT-PCR and plaque assays. We observed significantly lower levels of viral replication in the lung tissue of the ATV006-treated group (250 and 500 mg/kg) than in the control group (Fig. 3C and D). Similar results were obtained with plaque assays, showing that ATV006 treatment caused a dose-dependent decrease in the number of MHV infectious particles (Fig. 3E). Histopathological analysis of lung tissue

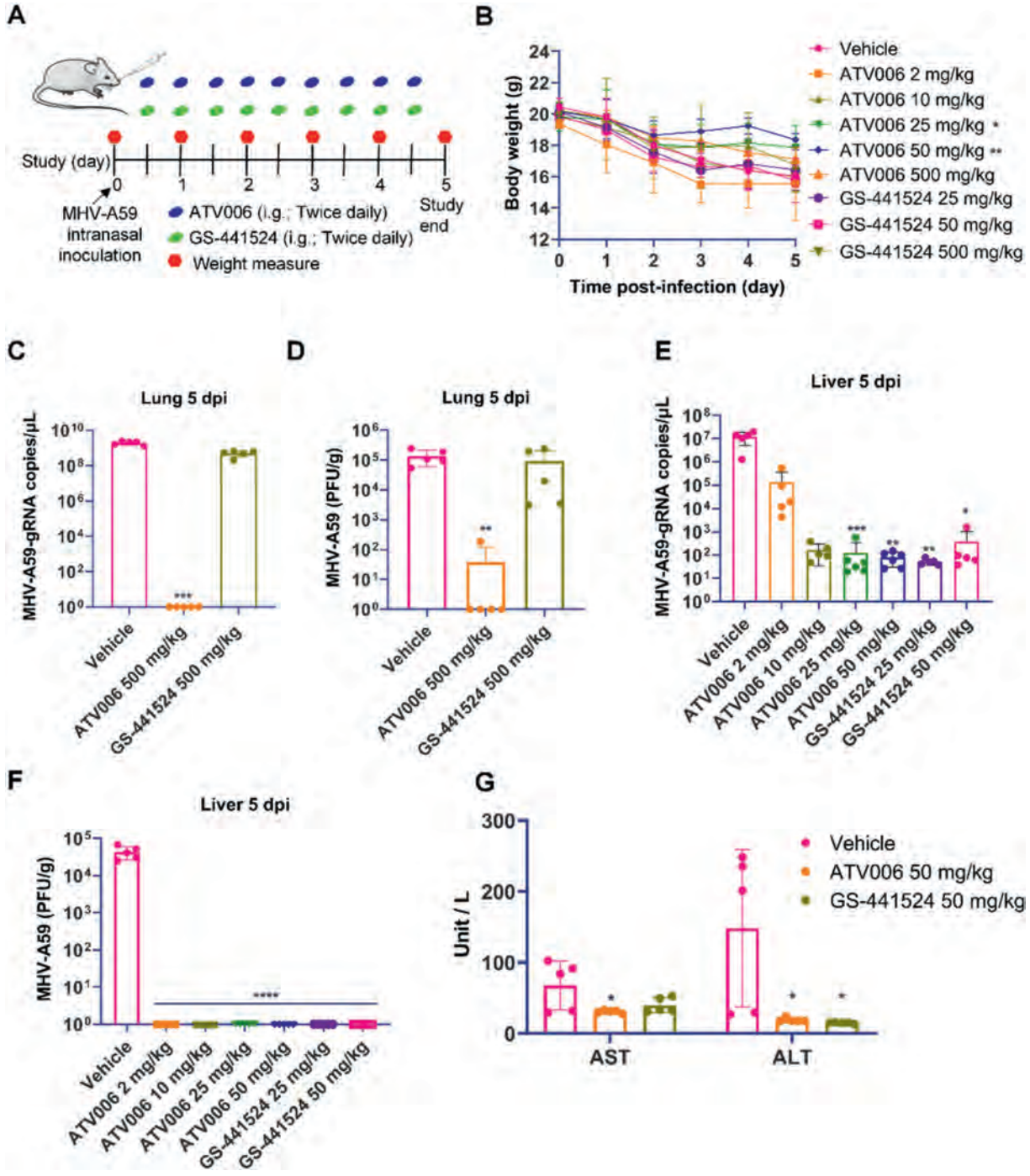

Figure 4 Therapeutic treatment of mice with ATV006 reduces MHV replication and pathology. BALB/c mice were intranasally inoculated with 4×10^5 PFU of MHV-A59 and divided into the following groups depending on treatment: vehicle ($n = 5$), ATV006 (500, 50, 25, 10, or 2 mg/kg, administered intragastric twice daily starting at 12 h post-infection (hpi), $n = 5-6$), and GS-441524 (500, 50, or 25 mg/kg, administered intragastric twice daily starting at 12 hpi, $n = 5$). (A) The time course of the experiment. (B) The change in mouse body weight over time after infection. (C, D) Viral abundance in the lung at 5 dpi as determined by qRT-PCR and plaque assay. (E, F) Viral abundance in the liver at 5 dpi as determined by qRT-PCR and plaque assay. (G) The levels of ALT and AST in the serum of mice from the indicated groups at 5 dpi. The data are expressed as mean ± SEM, $^*P < 0.05$; $^{**}P < 0.01$; $^{***}P < 0.001$; $^{****}P < 0.0001$ compared to the vehicle.

at 3 dpi revealed that vehicle-treated mice had more inflammatory cell infiltration compared to mice treated with ATV006 at 500 mg/kg (Fig. 3F). Furthermore, ATV006 significantly reduced the production of inflammatory cytokines and chemokines in the lung, including *Ifnβ*, *Cxcl10*, *Il6*, *Il1β*, and *Ifnγ* (Fig. 3G).

3.4. Therapeutic administration of ATV006 reduces MHV replication and pathogenesis

The fact that ATV006 showed potent antiviral activity and prevented mouse death in prophylactic dose-escalation studies (Figs. 2 and 3) prompted us to investigate its therapeutic potential. The experimental timeline is graphically presented in Fig. 4A. Compared to vehicle treatment, ATV006 treatment (25 and 50 mg/kg) initiated 12 h after intranasal MHV infection significantly reduced body weight loss. The weight loss was most effectively reduced in the therapeutic group that received 50 mg/kg of ATV006. The lack of effect in the 500 mg/kg group could be attributed to toxicity at this high drug concentration (Fig. 4B). Next, we evaluated the abundance of MHV in the lung and liver at 5 dpi by qRT-PCR and plaque assay (Fig. 4C−F). We compared the therapeutic effect of ATV006 on viral titers with that of GS-441524 at the same high dose of 500 mg/kg and found that only ATV006 significantly inhibited MHV replication in the lung (Fig. 4C and D). In the liver, therapeutic administration of ATV006 inhibited MHV replication in a dose-dependent manner (Fig. 4E). Furthermore, virus titers at 5 dpi were below the detection limit of the plaque assay in all treated groups (ATV006 at 2, 10, 25, 50, and GS-441524 at 25, 50 mg/kg; Fig. 4F). Serological tests revealed that therapeutic administration of ATV006 and GS-441524 (50 mg/kg) significantly reduced the liver injury markers ALT and AST compared to the vehicle group. This demonstrated that ATV006 was therapeutically effective in protecting mice from liver injury (Fig. 4G).

We then wanted to determine how late the ATV006 treatment could begin to maintain its effectiveness. For this purpose, ATV006 treatment (2, 10, 25, 50, 250, and 500 mg/kg) was initiated at 24, 48, 72, and 96 h post-infection (hpi). Thereafter, the drug was administered every 12 h (Fig. 5A). We assessed the abundance of MHV in the lung and liver at 5 dpi using qRT-PCR and plaque assays (Fig. 5B−E). Consistent with the results shown in Fig. 4, we observed that a higher dose of ATV006 was required to exert an antiviral effect in the lung than in the liver. In the lung, qRT-PCR revealed significant inhibition of viral replication only when ATV006 treatment (250 mg/kg) began no later than 24 hpi. Treatment with a higher dose of ATV006 (500 mg/kg) was effective when started within 48 hpi (Fig. 5B). Similar results were obtained in plaque assays. No infectious viral particles were detected in the lungs when ATV006 treatment (500 mg/kg) was initiated within 48 hpi (Fig. 5C). In the liver, various doses of ATV006 (10, 25, and 50 mg/kg) administered at 24 or 48 hpi significantly inhibited MHV replication (Fig. 5D). Only the low dose 2 mg/kg proved ineffective. Notably, 50 mg/kg of ATV006, even when administered as late as 96 hpi, reduced virus titers to levels undetectable by plaque assay (Fig. 5E). Finally, we compared the severity of pathological manifestations in the lung and liver between the ATV006-treated and control groups. ATV006 at 10 mg/kg significantly reduced liver piecemeal necrosis, bridging necrosis, circumscribed hepatic necrosis, and portal inflammation when administered at 24, 48, and 72 hpi (Fig. 5F). Similarly, ATV006 (500 mg/kg) administered at 24 hpi reduced pulmonary edema and monocyte and neutrophil infiltration. However, bleeding in the lungs did not improve significantly in the same group (Fig. 5G). ALT and AST levels indicated that ATV006 treatment at 10 mg/kg alleviated liver injury (Fig. 5H). As shown in the figure, the results of ATV006 treatments at different time points after viral infection indicate that the inhibitory effect of the ATV006 on the virus gradually weakens as the treatment is delayed. When the ATV006 is added to the cells simultaneously with the virus, concentrations of 50, 10, and 1 μmol/L all achieved over 99% inhibition. However, when the drug was administered 48 h after the viral infection, no inhibitory effect was observed (Supporting Information Fig. S4). Collectively, the above results show that ATV006 administration as late as 96 hpi is still effective in inhibiting MHV replication in the liver, but the drug should be administered earlier for respiratory infection.

3.5. Therapeutic ATV006 treatment is efficacious against HCoV-NL63 in K18-hACE2 mice

HCoV-NL63 is a common human coronavirus that was first identified in the Netherlands in 2004[38]. It primarily infects the upper respiratory tract and has been widely distributed across the globe. This virus enters host cells by binding to the angiotensin-converting enzyme 2 (ACE2) receptor similarly as that of SARS-CoV-2[39]. Infections with HCoV-NL63 have been confirmed worldwide, primarily causing respiratory tract infections[40,41]. Using the K18-hACE2 mouse model of HCoV-NL63 infection, we conducted a therapeutic efficacy study to determine whether ATV006 (500 mg/kg), GS-441524 (500 mg/kg), and RDV (25 mg/kg) would reduce viral replication and improve pathogenic outcomes at 12 hpi, as therapy initiated at this time point was most successful in the aforementioned MHV model (Fig. 4). Consistent with the *in vivo* data from the MHV model, a 500 mg/kg dose of ATV006 provided protection against clinical disease symptoms, including prevention of weight loss, reduction in lung viral load, and alleviation of lung inflammation (Fig. 6A−E). The experimental timeline is graphically presented in Fig. 6A. The 500 mg/kg dose of ATV006 effectively prevented weight loss in mice (Fig. 6B) and significantly reduced viral replication in the lungs (Fig. 6C and D). Furthermore, ATV006 showed greater improvement in overall lung pathology in mice compared to the GS-441524 and RDV treatment (Fig. 6E). Therefore, early treatment with a 500 mg/kg dose of ATV006 effectively prevents the pathogenic effects of HCoV-NL63 in mice.

4. Discussion

Since the beginning of the 21st century, the world has experienced three global health crises caused by coronavirus infections: SARS in 2002, MERS in 2012, and COVID-19 in 2019. Vaccines are considered an effective strategy for managing such crises and preventing their recurrence in the future. However, despite significant progress in vaccine development, the high mutation rate of coronaviruses remains a major challenge. For example, the omicron variant of SARS-CoV-2[42] was found to evade existing vaccines[43]. Antiviral therapies are an alternative approach, but viral diversity prevents the use of existing direct-acting antiviral (DAA) drugs as a universal treatment. Therefore, broad-spectrum antivirals are urgently needed to treat diseases caused by emerging and re-emerging viruses[44-46].

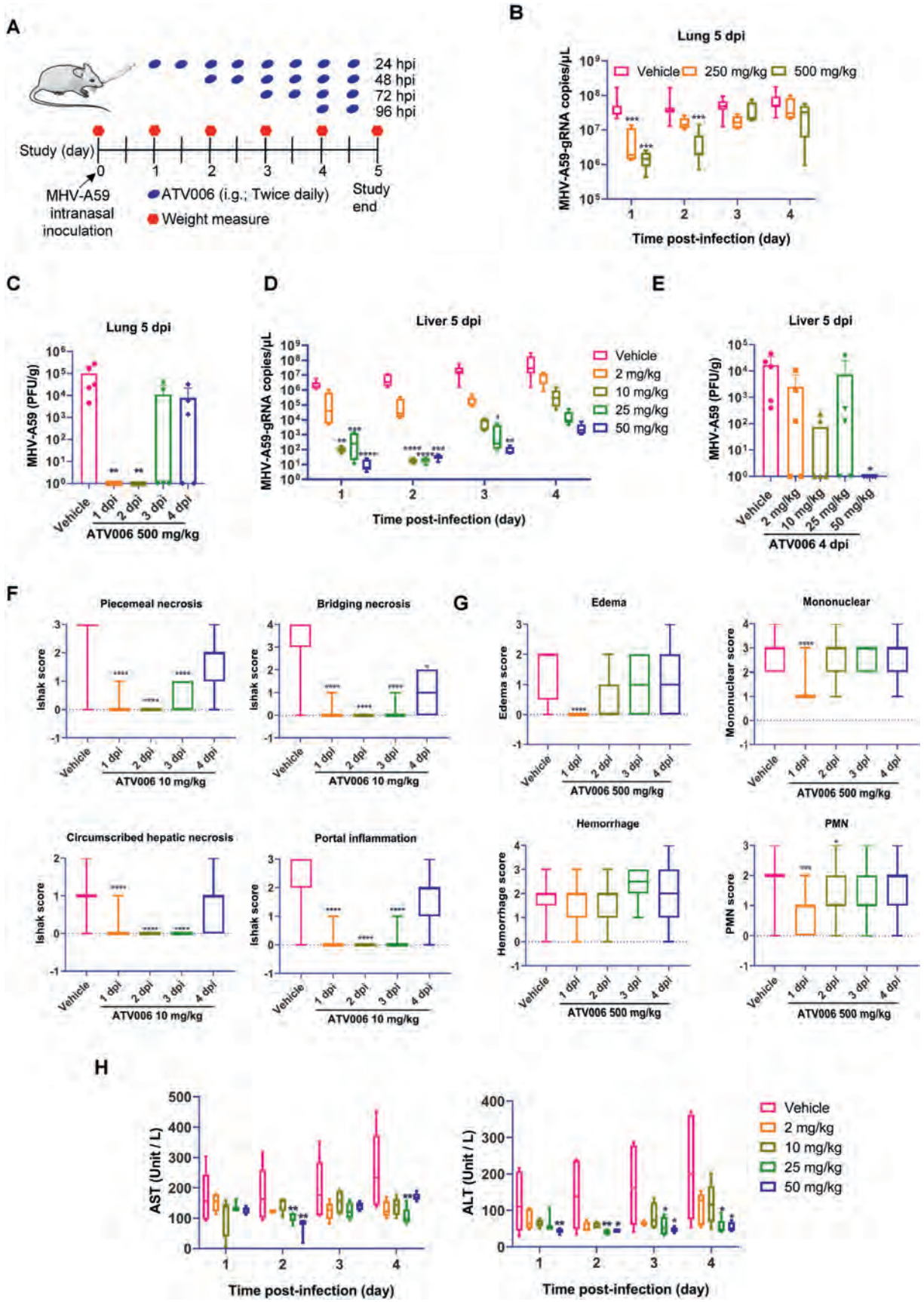

Figure 5 Therapeutic treatment of mice with ATV006 48 h after infection reduces viral replication and symptom severity. BALB/c mice were intranasally inoculated with 4×10^5 PFU of MHV-A59 and divided into the following groups depending on treatment: vehicle ($n = 5$) and

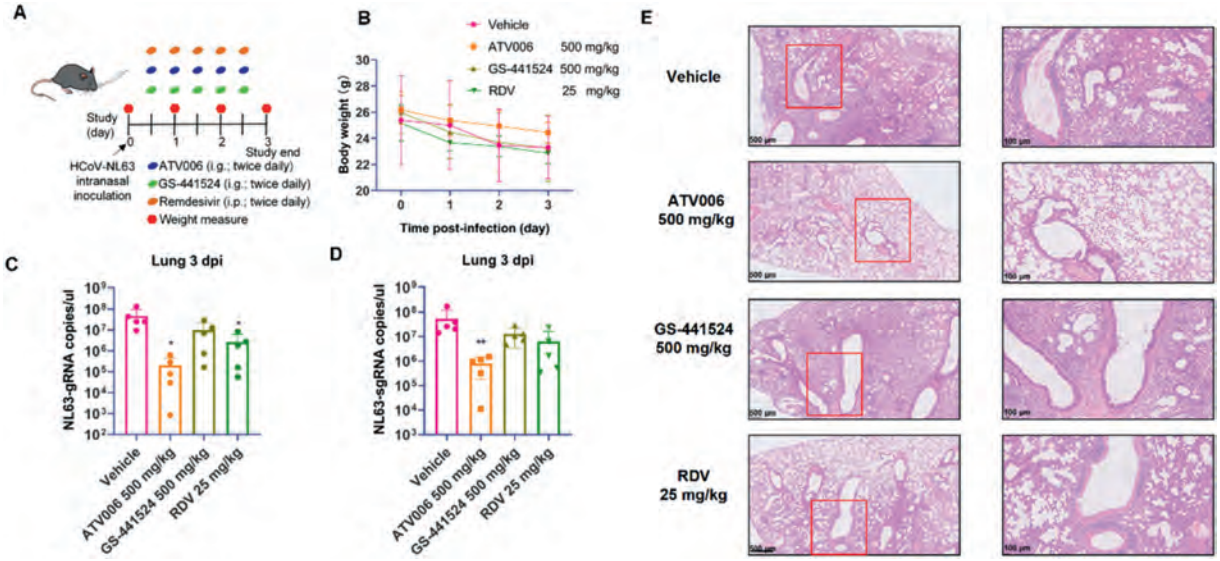

Figure 6 Therapeutic ATV006 treatment is efficacious against HCoV-NL63 in K18-hACE2 mice. K18-hACE2 mice were intranasally inoculated with 4×10^5 PFU of HCoV-NL63 and divided into the following groups depending on treatment: vehicle ($n = 5$), ATV006 (500 mg/kg, administered intragastric twice daily starting at 12 h post-infection (hpi), $n = 5$), and GS-441524 (500 mg/kg, administered intragastric twice daily starting at 12 hpi, $n = 5$). (A) The time course of the experiment. (B) The change in mouse body weight over time after infection. (C, D) Viral abundance in the lung at 3 dpi as determined by qRT-PCR. (E) Histopathological analysis of lung tissues from the vehicle group and the ATV006-treated group, GS-441524-treated group and RDV-treated group. The black bar is 500 μm (left panel) and 100 μm (right panel) at different magnifications. The red box in the low-magnification images indicates the magnified area for high-magnification images on the right panel (100 μm bar). The data are expressed as mean ± SEM, $*P < 0.05$; $**P < 0.01$.

Highly conserved and functionally indispensable viral proteins represent the most promising targets for broad-spectrum antiviral drugs. One such protein is the spike (S) protein of SARS-CoV-2, for which vaccines and antibody-based therapies have been developed[47,48]. However, the presence of mutational hotspots in the S protein, such as D614G[49], N501Y[50], and P681H[51], limits the efficacy of these therapeutic approaches. In contrast, the RdRP is not only highly conserved among coronaviruses (Supporting Information Fig. S5) but also has a low mutation rate, making it a promising target for drug development[11-13]. A number of SARS-CoV-2 RdRp inhibitors have been developed, including remdesivir[52], molnupiravir[16,53], VV116[17,54], and azvudine[18]. Some of these molecules have been found to have antiviral activity against other coronaviruses, such as SARS-CoV and MERS-CoV[16,24].

ATV006, the 5′-hydroxyl-isobutyryl prodrug of GS-441524, was originally discovered in our laboratory [19]. The compound is currently in Phase III clinical trials conducted by Gilead Sciences Inc. (Clinical Trials Identifier: NCT05715528). We have previously shown that ATV006 has excellent oral bioavailability in both rats and cynomolgus monkeys, as well as potent antiviral activity against several SARS-CoV-2 VOCs *in vitro* and in three mouse models[19]. In this study, we extend these findings by demonstrating that ATV006 has potent and broad-spectrum antiviral activity against human (HCoV-229E, OC43, and NL63) and animal (MHV, FIPV, CCoV, PEDV, TEGV, and SADS) coronaviruses (Fig. 1).

ATV006 and remdesivir share the same mechanism of action. Both ATV006 and remdesivir are prodrugs that are converted to GS-441524, but *via* different enzymatic pathways. Therefore, it is of interest to know whether the previously identified remdesivir binding sites[55] are conserved across the RdRp amino acid sequences of human and animal coronaviruses. Phylogenetic analysis revealed a high degree of conservation of remdesivir binding sites, specifically K500, S501, K545, V557, D623, S682, and S814 (Figs. S4−S6). This suggests that multiple coronaviruses are susceptible to both remdesivir and ATV006, highlighting the potential of ATV006 as a broad-spectrum anti-coronavirus drug.

We have previously reported that ATV006 has antiviral activity in several mouse models of SARS-CoV-2 infection[19]. SARS-CoV-2 uses the human angiotensin-converting enzyme 2 (hACE2) as an entry receptor. Due to differences between mouse and human ACE2 genes, inbred mouse strains are unable to support efficient SARS-CoV-2 infection[56-60]. To address this issue, several hACE2-expressing mouse models and viral-mediated hACE2 delivery systems have been developed[61-64]. However, these models are not without limitations. For example, adenovirus-mediated expression of human ACE2 causes obesity in mice, making this model

ATV006 (500, 250, 50, 25, 10, or 2 mg/kg, administered intragastric twice daily starting at 24, 48, 72, or 96 hpi, $n = 5$). (A) The time course of the experiment. (B, C) Viral abundance in the lung at 5 dpi as determined by qRT-PCR and plaque assay. (D, E) Viral abundance in the liver at 5 dpi as determined by qRT-PCR and plaque assay. (F) Histological features of acute hepatitis in the indicated groups. Three randomly chosen high-power (200 ×) fields of diseased liver were assessed per mouse at 5 dpi and blindly scored using the Ishak scoring system. (G) Edema, mononuclear infiltration, hemorrhage, and polymorphonuclear leukocyte (PMN) infiltration in the lungs of the indicated groups at 5 dpi. A score of 0 indicates the absence of the phenomenon, whereas a score of 4 indicates lesions in more than 66% of the lung area. (H) The levels of ALT and AST in the serum of mice from the indicated groups at 5 dpi. The data are expressed as mean ± SEM, $*P < 0.05$; $**P < 0.01$; $***P < 0.001$; $****P < 0.0001$ compared to the vehicle.

unsuitable for studying the relationship between obesity-related morbidities such as diabetes and COVID-19[65]. Similarly, K18-hACE2 mice develop fatal viral encephalitis due to SARS-CoV-2 neuroinvasion[66]. Thus, artificially humanized mice are not the best candidates for the development of pan-coronavirus inhibitors, and animal models of natural infection are better suited for this purpose. Mouse hepatitis virus (MHV), a member of the coronavirus family[67,68], infects the liver, lungs, and brain of mice, causing acute hepatitis, encephalitis, and chronic demyelinating disease[36,69]. The MHV-infected mice are a well-established model for the study of coronavirus replication and the development of pan-coronavirus drugs[70]. Consistent with our previous findings for SARS-CoV-2[19], both prophylactic and therapeutic administration of ATV006 demonstrated potent antiviral activity in mice challenged with MHV. Most importantly, ATV006 was able to inhibit MHV replication in the mouse liver as late as 96 h after infection (Fig. 5E). Although ATV006 showed strong antiviral activity in the liver, it was somewhat less effective in the lung (Figs. 4 and 5). This may be due to differences in drug distribution and metabolism in different organs. In line with this, the concentrations of the monophosphate and active triphosphate forms of ATV006 were significantly higher in the liver than in the lung[19,71]. Finally, the fact that ATV006 has potent inhibitory activity against several animal coronaviruses other than MHV suggests that this molecule may have veterinary applications. For example, ATV006 may be used in companion animal therapy and livestock management.

5. Conclusions

In conclusion, our results show that ATV006 has broad anti-coronavirus activity. It exhibits a good oral bioavailability and is effective against both human and animal coronaviruses, making it a promising oral therapy. The drug is highly effective in both prevention and treatment and is potentially useful in the fight against SARS-CoV-2, other human and animal coronaviruses, and emerging viruses in the future.

Acknowledgments

We thank Dr. Huanle Luo and the staff of the Biosafety Level 2 (BSL-2) facility of Sun Yat-sen University (Shenzhen) for their help in human coronavirus experiments. The study was supported by the National Natural Science Foundation of China (No. 82394461 and 32200108), the major project of Guangzhou National Laboratory (Grant No. GZNL2023A01008, China), and Shenzhen Science and Technology Program (No. JSGG20210901145403012 and JSGG20200225150431472, China).

Author contributions

Tiefeng Xu: Writing − review & editing, Writing − original draft, Visualization, Software, Methodology, Investigation, Formal analysis, Data curation. Kun Li: Original draft, Formal analysis, Data curation. Siyao Huang: Formal analysis, Data curation. Konstantin I. Ivanov: Writing − review & editing. Sidi Yang, Yanxi Ji, Hanwei Zhang, Wenbin Wu, Ye He, Qiang Zeng: Validation. Feng Cong, Qifan Zhou, Yingjun Li, Jian Pan, Jincun Zhao, Chunmei Li, Xumu Zhang: Resource. Liu Cao, Deyin Guo: Writing - review & editing, Writing - original draft, Supervision, Project administration, Funding acquisition, Conceptualization.

Conflicts of interest

The authors declare no conflicts of interest.

Appendix A. Supporting information

Supporting information to this article can be found online at https://doi.org/10.1016/j.apsb.2025.02.028.

References

1. Zhou H, Ni WJ, Huang W, Wang Z, Cai M, Sun YC. Advances in pathogenesis, progression, potential targets and targeted therapeutic strategies in SARS-CoV-2-induced COVID-19. *Front Immunol* 2022;**13**:834942.
2. Chen Y, Liu Q, Guo D. Emerging coronaviruses: genome structure, replication, and pathogenesis. *J Med Virol* 2020;**92**:418−23.
3. Liu Y, Chen D, Wang Y, Li X, Qiu Y, Zheng M, et al. Characterization of CCoV-HuPn-2018 spike protein-mediated viral entry. *J Virol* 2023; **97**:e0060123.
4. Akinloye OM, Rönkkö E, Savolainen-Kopra C, Ziegler T, Iwalokun BA, Deji-Agboola MA, et al. Specific viruses detected in nigerian children in association with acute respiratory disease. *J Trop Med* 2011;**2011**:690286.
5. Vlasova AN, Diaz A, Damtie D, Xiu L, Toh TH, Lee JS, et al. Novel canine coronavirus isolated from a hospitalized patient with pneumonia in East Malaysia. *Clin Infect Dis* 2022;**74**:446−54.
6. Lednicky JA, Tagliamonte MS, White SK, Elbadry MA, Alam MM, Stephenson CJ, et al. Independent infections of porcine deltacoronavirus among Haitian children. *Nature* 2021;**600**:133−7.
7. Ksiazek TG, Erdman D, Goldsmith CS, Zaki SR, Peret T, Emery S, et al. A novel coronavirus associated with severe acute respiratory syndrome. *N Engl J Med* 2003;**348**:1953−66.
8. Li Q, Guan X, Wu P, Wang X, Zhou L, Tong Y, et al. Early transmission dynamics in wuhan, China, of novel coronavirus-infected pneumonia. *N Engl J Med* 2020;**382**:1199−207.
9. Zaki AM, van Boheemen S, Bestebroer TM, Osterhaus AD, Fouchier RA. Isolation of a novel coronavirus from a man with pneumonia in Saudi Arabia. *N Engl J Med* 2012;**367**:1814−20.
10. Zhong NS, Zheng BJ, Li YM, Poon LLM, Xie ZH, Chan KH, et al. Epidemiology and cause of severe acute respiratory syndrome (SARS) in Guangdong, People's Republic of China, in February, 2003. *Lancet* 2003;**362**:1353−8.
11. Hillen HS, Kokic G, Farnung L, Dienemann C, Tegunov D, Cramer P. Structure of replicating SARS-CoV-2 polymerase. *Nature* 2020;**584**: 154−6.
12. Gao Y, Yan L, Huang Y, Liu F, Zhao Y, Cao L, et al. Structure of the RNA-dependent RNA polymerase from COVID-19 virus. *Sci (New York, NY)* 2020;**368**:779−82.
13. Kokic G, Hillen HS, Tegunov D, Dienemann C, Seitz F, Schmitzova J, et al. Mechanism of SARS-CoV-2 polymerase stalling by remdesivir. *Nat Commun* 2021;**12**:279.
14. Goldman JD, Lye DCB, Hui DS, Marks KM, Bruno R, Montejano R, et al. Remdesivir for 5 or 10 days in patients with severe Covid-19. *N Engl J Med* 2020;**383**:1827−37.
15. Kabinger F, Stiller C, Schmitzová J, Dienemann C, Kokic G, Hillen HS, et al. Mechanism of molnupiravir-induced SARS-CoV-2 mutagenesis. *Nat Struct Mol Biol* 2021;**28**:740−6.
16. Wahl A, Gralinski LE, Johnson CE, Yao W, Kovarova M, Dinnon 3rd KH, et al. SARS-CoV-2 infection is effectively treated and prevented by EIDD-2801. *Nature* 2021;**591**:451−7.
17. Shen Y, Ai J, Lin N, Zhang H, Li Y, Wang H, et al. An open, prospective cohort study of VV116 in Chinese participants infected with SARS-CoV-2 omicron variants. *Emerg Microbes Infect* 2022;**11**:1518−23.
18. Zhang JL, Li YH, Wang LL, Liu HQ, Lu SY, Liu Y, et al. Azvudine is a thymus-homing anti-SARS-CoV-2 drug effective in treating COVID-19 patients. *Signal Transduct Target Ther* 2021;**6**:414.

19. Cao L, Li Y, Yang S, Li G, Zhou Q, Sun J, et al. The adenosine analog prodrug ATV006 is orally bioavailable and has preclinical efficacy against parental SARS-CoV-2 and variants. *Sci Transl Med* 2022;**14**: eabm7621.
20. Sheahan TP, Sims AC, Graham RL, Menachery VD, Gralinski LE, Case JB, et al. Broad-spectrum antiviral GS-5734 inhibits both epidemic and zoonotic coronaviruses. *Sci Transl Med* 2017;**9**:eaal3653.
21. Malin JJ, Suárez I, Priesner V, Fätkenheuer G, Rybniker J. Remdesivir against COVID-19 and other viral diseases. *Clin Microbiol Rev* 2020; **34**:e00162-20.
22. Lo MK, Shrivastava-Ranjan P, Chatterjee P, Flint M, Beadle JR, Valiaeva N, et al. Broad-spectrum *in vitro* antiviral activity of ODBG-P-RVn: an orally-available, lipid-modified monophosphate prodrug of remdesivir parent nucleoside (GS-441524). *Microbiol Spectr* 2021;**9**: e0153721.
23. Al-Beltagi S, Preda CA, Goulding LV, James J, Pu J, Skinner P, et al. Thapsigargin is a broad-spectrum inhibitor of major human respiratory viruses: coronavirus, respiratory syncytial virus and influenza A virus. *Viruses* 2021;**13**:234.
24. Li Y, Liu M, Yan Y, Wang Z, Dai Q, Yang X, et al. Molnupiravir and its active form, EIDD-1931, show potent antiviral activity against enterovirus infections *in vitro* and *in vivo*. *Viruses* 2022;**14**:1142.
25. Painter WP, Holman W, Bush JA, Almazedi F, Malik H, Eraut N, et al. Human safety, tolerability, and pharmacokinetics of molnupiravir, a novel broad-spectrum oral antiviral agent with activity against SARS-CoV-2. *Antimicrob Agents Chemother* 2021;**65**:e02428-20.
26. Yang Y, Cao L, Yan M, Zhou J, Yang S, Xu T, et al. Synthesis of deuterated S-217622 (Ensitrelvir) with antiviral activity against coronaviruses including SARS-CoV-2. *Antivir Res* 2023;**213**:105586.
27. Li Y, Cao L, Li G, Cong F, Li Y, Sun J, et al. Remdesivir metabolite GS-441524 effectively inhibits SARS-CoV-2 infection in mouse models. *J Med Chem* 2022;**65**:2785−93.
28. Andrade A, Campolina-Silva GH, Queiroz-Junior CM, de Oliveira LC, Lacerda LSB, Pimenta JC, et al. A iBiosafety level 2 mouse model for studying betacoronavirus-induced acute lung damage and systemic manfestations. *J Virol* 2021;**95**:e0127621.
29. Zhong WJ, Yang HH, Guan XX, Xiong JB, Sun CC, Zhang CY, et al. Inhibition of glycolysis alleviates lipopolysaccharide-induced acute lung injury in a mouse model. *J Cel Physiol* 2019;**234**:4641−54.
30. Kim U, Kim N, Shin HY. Modeling non-alcoholic fatty liver disease (NAFLD) using "Good-Fit" genome-editing tools. *Cells* 2020;**9**:2572.
31. Beitz E. TEXshade: shading and labeling of multiple sequence alignments using LATEX2 epsilon. *Bioinformatics* 2000;**16**:135−9.
32. Zhang Y, Chan S, He R, Liu Y, Song X, Tu ZC, et al. 1-Methyl-3-((4-(quinolin-4-yloxy)phenyl)amino)-1*H*-pyrazole-4-carboxamide derivatives as new rearranged during Transfection (RET) kinase inhibitors capable of suppressing resistant mutants in solvent-front regions. *Eur J Med Chem* 2022;**244**:114862.
33. Xu X, Zhang Q, Wang X, Jin J, Wu C, Feng L, et al. Discovery of a potent and highly selective inhibitor of SIRT6 against pancreatic cancer metastasis *in vivo*. *Acta Pharm Sin B* 2024;**14**:1302−16.
34. Fung TS, Liu DX. Human coronavirus: host-pathogen interaction. *Annu Rev Microbiol* 2019;**73**:529−57.
35. Kesheh MM, Hosseini P, Soltani S, Zandi M. An overview on the seven pathogenic human coronaviruses. *Rev Med Virol* 2022;**32**: e2282.
36. Yang Z, Du J, Chen G, Zhao J, Yang X, Su L, et al. Coronavirus MHV-A59 infects the lung and causes severe pneumonia in C57BL/6 mice. *Virol Sin* 2014;**29**:393−402.
37. Corman VM, Muth D, Niemeyer D, Drosten C. Hosts and sources of endemic human coronaviruses. *Adv Virus Res* 2018;**100**:163−88.
38. van der Hoek L, Pyrc K, Jebbink MF, Vermeulen-Oost W, Berkhout RJ, Wolthers KC, et al. Identification of a new human coronavirus. *Nat Med* 2004;**10**:368−73.
39. Hofmann H, Pyrc K, van der Hoek L, Geier M, Berkhout B, Pöhlmann S. Human coronavirus NL63 employs the severe acute respiratory syndrome coronavirus receptor for cellular entry. *Proc Natl Acad Sci U S A* 2005;**102**:7988−93.
40. van der Hoek L, Sure K, Ihorst G, Stang A, Pyrc K, Jebbink MF, et al. Croup is associated with the novel coronavirus NL63. *Plos Med* 2005; **2**:e240.
41. Abdul-Rasool S, Fielding BC. Understanding human coronavirus HCoV-NL63. *Open Virol J* 2010;**4**:76−84.
42. Shuai H, Chan JF, Hu B, Chai Y, Yuen TT, Yin F, et al. Attenuated replication and pathogenicity of SARS-CoV-2 B.1.1.529 omicron. *Nature* 2022;**603**:693−9.
43. Cao Y, Yisimayi A, Jian F, Song W, Xiao T, Wang L, et al. BA.2.12.1, BA.4 and BA.5 escape antibodies elicited by omicron infection. *Nature* 2022;**608**:593−602.
44. Debing Y, Neyts J, Delang L. The future of antivirals: broad-spectrum inhibitors. *Curr Opin Infect Dis* 2015;**28**:596−602.
45. Gao GF. From "A"IV to "Z"IKV: attacks from emerging and re-emerging pathogens. *Cell* 2018;**172**:1157−9.
46. Zhu JD, Meng W, Wang XJ, Wang HC. Broad-spectrum antiviral agents. *Front Microbiol* 2015;**6**:517.
47. Li M, Wang H, Tian L, Pang Z, Yang Q, Huang T, et al. COVID-19 vaccine development: milestones, lessons and prospects. *Signal Transduct Target Ther* 2022;**7**:146.
48. Tregoning JS, Flight KE, Higham SL, Wang Z, Pierce BF. Progress of the COVID-19 vaccine effort: viruses, vaccines and variants *versus* efficacy, effectiveness and escape. *Nat Rev Immunol* 2021;**21**:626−36.
49. Korber B, Fischer WM, Gnanakaran S, Yoon H, Theiler J, Abfalterer W, et al. Tracking changes in SARS-CoV-2 spike: evidence that D614G increases infectivity of the COVID-19 virus. *Cell* 2020; **182**:812−27.e19.
50. Liu Y, Liu J, Plante KS, Plante JA, Xie X, Zhang X, et al. The N501Y spike substitution enhances SARS-CoV-2 infection and transmission. *Nature* 2022;**602**:294−9.
51. Lubinski B, Fernandes MHV, Frazier L, Tang T, Daniel S, Diel DG, et al. Functional evaluation of the P681H mutation on the proteolytic activation of the SARS-CoV-2 variant B.1.1.7 (Alpha) spike. *iScience* 2022;**25**:103589.
52. Hong YN, Xu J, Sasa GBK, Zhou KX, Ding XF. Remdesivir as a broad-spectrum antiviral drug against COVID-19. *Eur Rev Med Pharmacol Sci* 2021;**25**:541−8.
53. Cox RM, Wolf JD, Plemper RK. Therapeutically administered ribonucleoside analogue MK-4482/EIDD-2801 blocks SARS-CoV-2 transmission in ferrets. *Nat Microbiol* 2021;**6**:11−8.
54. Xie Y, Yin W, Zhang Y, Shang W, Wang Z, Luan X, et al. Design and development of an oral remdesivir derivative VV116 against SARS-CoV-2. *Cell Res* 2021;**31**:1212−4.
55. Wang Q, Wu J, Wang H, Gao Y, Liu Q, Mu A, et al. Structural basis for RNA replication by the SARS-CoV-2 polymerase. *Cell* 2020;**182**: 417−28.e13.
56. Letko M, Marzi A, Munster V. Functional assessment of cell entry and receptor usage for SARS-CoV-2 and other lineage B betacoronaviruses. *Nat Microbiol* 2020;**5**:562−9.
57. Li F, Li W, Farzan M, Harrison SC. Structure of SARS coronavirus spike receptor-binding domain complexed with receptor. *Sci (New York, NY)* 2005;**309**:1864−8.
58. Li W, Moore MJ, Vasilieva N, Sui J, Wong SK, Berne MA, et al. Angiotensin-converting enzyme 2 is a functional receptor for the SARS coronavirus. *Nature* 2003;**426**:450−4.
59. Walls AC, Park YJ, Tortorici MA, Wall A, McGuire AT, Veesler D. Structure, function, and antigenicity of the SARS-CoV-2 spike glycoprotein. *Cell* 2020;**181**:281−92.e6.
60. Yan R, Zhang Y, Li Y, Xia L, Guo Y, Zhou Q. Structural basis for the recognition of SARS-CoV-2 by full-length human ACE2. *Sci (New York, NY)* 2020;**367**:1444−8.
61. Hassan AO, Case JB, Winkler ES, Thackray LB, Kafai NM, Bailey AL, et al. A SARS-CoV-2 infection model in mice demonstrates protection by neutralizing antibodies. *Cell* 2020;**182**:744−53.e4.
62. Israelow B, Song E, Mao T, Lu P, Meir A, Liu F, et al. Mouse model of SARS-CoV-2 reveals inflammatory role of type I interferon signaling. *bioRxiv* 2020. Available from: https://doi.org/10.1101/2020.05.27.118893.

63. Sun SH, Chen Q, Gu HJ, Yang G, Wang YX, Huang XY, et al. A mouse model of SARS-CoV-2 infection and pathogenesis. *Cell Host Microbe* 2020;**28**:124−33.e4.
64. McCray Jr PB, Pewe L, Wohlford-Lenane C, Hickey M, Manzel L, Shi L, et al. Lethal infection of K18-hACE2 mice infected with severe acute respiratory syndrome coronavirus. *J Virol* 2007;**81**:813−21.
65. Rai P, Chuong C, LeRoith T, Smyth JW, Panov J, Levi M, et al. Adenovirus transduction to express human ACE2 causes obesity-specific morbidity in mice, impeding studies on the effect of host nutritional status on SARS-CoV-2 pathogenesis. *Virology* 2021;**563**: 98−106.
66. Kumari P, Rothan HA, Natekar JP, Stone S, Pathak H, Strate PG, et al. Neuroinvasion and encephalitis following intranasal inoculation of SARS-CoV-2 in K18-hACE2 mice. *Viruses* 2021;**13**:132.
67. Lai MM, Stohlman SA. RNA of mouse hepatitis virus. *J Virol* 1978; **26**:236−42.
68. Cheever FS, Daniels JB, Pappenheimer AM, Bailey OT. A murine virus (JHM) causing disseminated encephalomyelitis with extensive destruction of myelin. *J Exp Med* 1949;**90**:181−210.
69. Weiss SR, Leibowitz JL. Coronavirus pathogenesis. *Adv Virus Res* 2011;**81**:85−164.
70. Körner RW, Majjouti M, Alcazar MAA, Mahabir E. Of mice and men: the coronavirus MHV and mouse models as a translational approach to understand SARS-CoV-2. *Viruses* 2020;**12**:880−8.
71. Hu WJ, Chang L, Yang Y, Wang X, Xie YC, Shen JS, et al. Pharmacokinetics and tissue distribution of remdesivir and its metabolites nucleotide monophosphate, nucleotide triphosphate, and nucleoside in mice. *Acta Pharmacol Sin* 2021;**42**:1195−200.